ISSN: 2688-8645

Fuzzy Adaptive Finite-time Control of Stabilized Platform in Rotary Steerable System with Sensor and Actuator Failures

Min Wan [1], Qi Cen [1] and Lifang Zhou [2]

[1] School of Mechanical and Electrical Engineering, Southwest Petroleum University, Chengdu, Sichuan, 610500, China

[2] Department of Mechanical and Electrical Engineering, Jiangsu Jiangyin Secondary Vocational School, Jiangyin, Jiangsu, 214431, China

Abstract

This paper investigates the tracking control problem of a stable platform with a rotating guidance system that has sensor and actuator failures. In order to improve the robustness of the angle control of rotary steering system drilling tools, a fuzzy adaptive finite-time control is proposed. Compared with existing control strategies, this paper integrates dynamic surface control technology and finite-time technology through adaptive fuzzy backstepping control to address the trajectory tracking problem of a rotating guidance system with simultaneous sensor and actuator failures. A fuzzy state observer is designed to observe unobservable states in the system. Then, based on the Lyapunov function, a signal compensation mechanism is constructed, and an adaptive law is designed to estimate unknown fault parameters, thereby reducing the impact of sensor failure faults on tracking performance. The proposed control method can simultaneously compensate for actuator and sensor faults, ensuring that the tracking error converges to a small neighborhood near the origin within a finite time, thereby improving the stability and safety of the system. Simulation results validate the effectiveness of this control method.

Keywords

Rotary Guidance Systems; Stabilized Platform; Sensor and Actuator Failures; Adaptive Fuzzy Backstepping Control; Finite Time Control.

1. Introduction

With the deepening of oil and gas exploration and development, the development field gradually expands from conventional oil and gas resources to unconventional oil and gas resources. Not only is the extraction environment harsher, but also the borehole quality requirements are higher, which greatly increases the difficulty of oil and gas resources development. [1] Rotary guidance system is an advanced directional drilling technology, which has the advantages of low cost, smooth borehole trajectory, good borehole quality and high degree of trajectory control automation. [2] As the key component of guidance control in the system, the core task of the stabilized platform is to adjust the angle of the tool face to ensure that the whole system can move stably in the preset direction. [3]

During the drilling process, the rotary guidance system ensures that the borehole trajectory is drilled at a set angle, and the key technology to achieve this is to achieve stable control of the stabilized platform at any given angle. [4] The tool face is an important parameter for borehole trajectory control and is used to describe the orientation of the drill bit. The stabilized platform located inside the drill collar is used to control the biasing unit to generate the biasing force to adjust the tool face angle. As there are many uncertainties and unknown disturbances in the actual working environment, the stabilized platform needs to overcome the disturbances and

ISSN: 2688-8645

maintain the stability of the whole system, so that the system can accurately track a given deviation of the tool face angle. [5] Therefore, as the 'brain' of the downhole guidance tool, accurate tool face control of the stabilized platform is essential to ensure that the drilling system operates in accordance with the established trajectory.

In complex underground geological environments, control systems generally face problems such as severe vibration, unknown disturbances, and complex rig motions. Therefore, many advanced control strategies are also applied to the control of rotary guided stabilized platforms. Zhang et al.,[6] employed a fuzzy method based on backpropagation neural networks to control the trajectory tracking of rotary steerable systems. Wang et al.,[7] utilized a composite control algorithm—minor hole deviation control and major hole deviation control—to address trajectory tracking control for rotary steerable systems. Ji et al.,[8] established an exponential impulsive control function based on PID control and angular position error sliding mode control strategies, achieving rapid and accurate tool face angle tracking through closed-loop angular position control.

In practical engineering, due to the harsh downhole environment, the high temperature environment affects the electronic circuit, which can easily cause the sensor measurement failure. The drilling fluid inevitably contains solid particles, iron filings and other debris, and is prone to enter the bearing part of the motor, and the friction is exacerbated, leading to motor jamming or motor failure. In Wang et al., [9] proposed an adaptive enhanced state observer to simultaneously estimate system state, sensor, and actuator faults. A new expected weight and PI-type fuzzy feedback fault-tolerant controller based on sensor fault estimation information aims to simultaneously compensate for the effects of sensor and actuator faults.

Based on the above analysis, this paper proposes a fuzzy adaptive finite-time control method for trajectory tracking of the Rotary Steerable System (RSS) stable platform subject to sensor and actuator faults. The main contributions of this work are summarized as follows:

1. A finite-time fuzzy adaptive fault-tolerant control framework is established for the RSS stable platform. This framework explicitly accounts for simultaneous sensor faults, actuator faults, and unmeasurable system states.

2. To address partial sensor faults, adaptive parameters are designed to actively compensate for fault effects. The proposed adaptive fuzzy control scheme not only maintains system stability under concurrent sensor and actuator faults but also demonstrates robust adaptability.

3. The integration of finite-time techniques with adaptive control guarantees that the tracking error converges to a small neighborhood of the origin within a finite time, which improves the convergence rate and transient performance.

2. System Modelling

2.1. Stabilized Platform Structure

The stabilized platform is suspended inside the drill collar by means of upper and lower support bearings and can rotate independently of the collar. The platform can be considered as a rigid cylinder. [10] The platform includes all the components on the left side of the upper valve, as shown in Figure 1.

The rotary steering system stabilization platform is a module that is unaffected by the rotation of the drill pipe and drill collar. Its function is to ensure that the drilling tools maintain a specific tool face angle as required. As illustrated in Figure l, two turbine generators are installed at opposite ends of the platform. The upper turbine generator generates electrical energy to ensure the platform operates normally. When drilling fluid flows through the upper turbine generator, the motor rotor rotates under force, generating an electromotive force, which is then rectified and stabilized before being supplied to the stabilization platform. The lower turbine

ISSN: 2688-8645

upper valve to suspend in the designated direction. At this point, the entire stable platform is maintained at the designated tool face position. [11]

The electronics module is the electronic control core of the stabilized platform and has the function of implementing downhole closed-loop control, in addition to data measurement and communication with the surface. Located between the platform's two turbine generators, the electronics bay integrates modules for control, detection and communication circuits. All the equipment is encased in a metal cylinder, hence the name electronics bay.

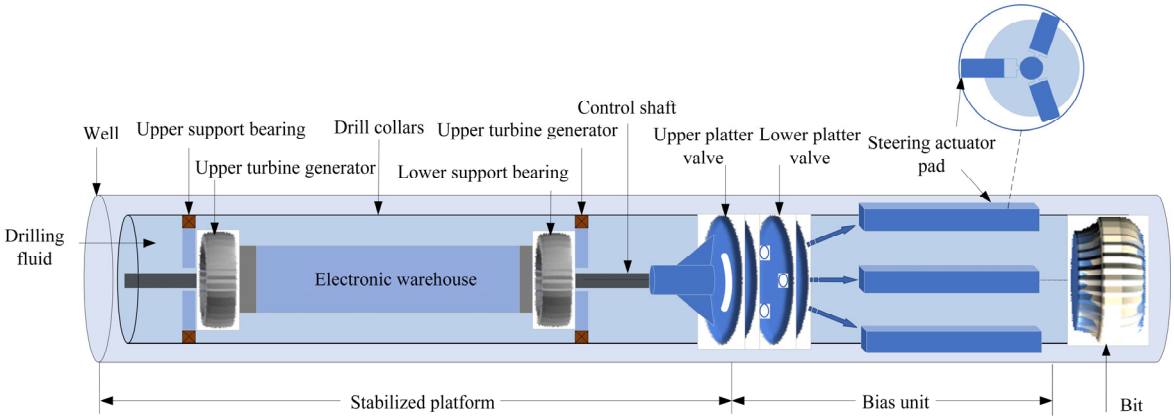

Figure 1. Stabilized platform structure schematic diagram

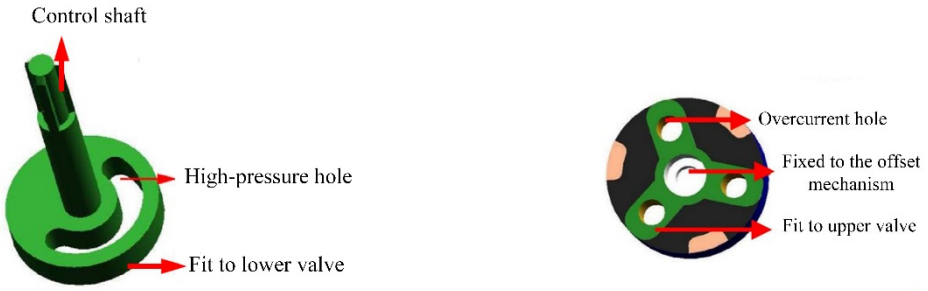

a) Structure of the upper valve b) Structure of the lower valve

Figure 2. Diagram illustrating the structure of the upper and lower valves

The upper valve is connected to the main shaft of the platform. A channel for drilling fluid to flow through is opened on the valve, also known as a high-pressure hole, as shown in Figure 2 (a). The lower valve is fixed to the bias unit and has the same direction of rotation as the drill collar; it has three evenly spaced holes and is connected to the steering slap on the drill collar through a water eye-mud channel, known as the overflow hole, as shown in Figure 2 (b). The lower valve rotates with the drill collar, and the structure of the upper and lower valves are connected when one or both of the holes above are turned to the high-pressure hole position of the upper valve. At this time, the drilling fluid will enter the overflow hole and subsequently push against the well wall through the channel-driven slap, and the whole drilling tool will be deflected in the direction of the opposite force to achieve the guiding function. The position of the upper disc valve determines the direction in which the guiding force is generated, and the position of the upper valve is essentially the position of the stabilized platform, so the core of the control is to control the position of the tool face of the stabilized platform.

The eccentricity moment of the platform is divided into two categories: one is the eccentricity moment caused by manufacturing and installation errors; the other is the additional moment of flexural deformation under the action of oscillatory impact.

ISSN: 2688-8645

The eccentricity moment due to manufacturing and installation errors can be divided into two types, one is the mass-distributed eccentricity moment M_g, which is expressed as follows

$$M_g = r_0 mg \sin\theta \sin\beta \tag{1}$$

The other is the mounting eccentric acting moment M_m, which can be expressed as

$$M_m = r_m mg \sin\theta \sin\beta \tag{2}$$

where θ is the tool face angle; β is the well inclination angle; r_0 is the eccentricity distance; r_m is the different axis error.

Combining Equation (1) and (2) yields the eccentric acting moment M_a, i.e.

$$\begin{aligned} M_a &= M_m + M_g \\ &= r_m mg \sin\theta \sin\beta + r_0 m_g g \sin\theta \sin\beta \\ &= f \sin\theta \end{aligned} \tag{3}$$

where f is the eccentricity moment equivalent coefficient, and at $\beta = 90°$, the value of $0 \sim 0.65\ N \cdot m$ is between.

For the additional moment of flexural deformation under oscillatory impact, the stabilized platform will undergo significant lateral flexural deformation under transverse impact loading. The transverse flexural deformation causes structural deformation of the platform, resulting in a moment that adversely affects the control of the platform tool surface. The platform can be viewed as a cylinder with uniformly distributed mass, which simplifies the complex flexural deformation problem to a simply supported beam flexural deformation problem under uniform loading. The simplified flexural deformation can be expressed as

$$\begin{aligned} M_r &= \int_0^L -\frac{mg}{L}\frac{px}{24EI}(2Lx^2 - x^3 - L^3)dx \sin\theta \sin\beta \\ &= 0.64 r_{1\max} \cdot mg \sin\theta \sin\beta \end{aligned} \tag{4}$$

where p is the distributed load of the equivalent vibration, E is the elastic modulus of the material, I is the moment of inertia, L is the overall length of the platform, θ is the well inclination angle, β is the tool face angle, and $r_{1\max}$ is the maximum deflection.

In Reference [11], Wang et al. provided equation (5) to represent the nonlinear dynamic equation of a stable platform

$$J\ddot{\theta} + k_1\dot{\theta} + f \sin\theta = M_0 + T(t) + \Delta(t) \tag{5}$$

where J is the rotational moment of inertia of the stabilized platform; k_1 is the viscous friction coefficient of the drilling fluid on the stabilized platform; f is the equivalent coefficient of the eccentricity moment; M_0 denotes the fixed moment independent of time; the total disturbance moment $\Delta(t)$ can be expressed as the sum of the three disturbance moments, denoted by $\Delta(t) = \Delta_1(t) + \Delta_2(t) + \Delta_3(t)$, where moment $\Delta_1(t)$ is the dynamic friction moment of the upper and lower disc valves, and it can be written as a cosine function, i.e. $\Delta_1(t) = b\cos(\omega \cdot t)$; moment $\Delta_2(t)$ is the hydrodynamic impact moment, and it is a random perturbation with a mean value of 0, denoted by . is a positive and negative square wave pulse with mean value 0; moment $\Delta_3(t)$ is the additional moment of flexural deformation in the eccentricity moment, which is set as a random disturbance with mean value 0, denoted as $\Delta_3(t) = A \cdot rand(t)$. $\ddot{\theta}$ and $\dot{\theta}$ are the angular acceleration and angular velocity of the steady walking platform, respectively.

ISSN: 2688-8645

2.2. Stable Platform Tool Face Angle Control System Structural Design

The tool face angle control system for the stabilization platform comprises a controller, an analog-to-digital converter, a PWM pulse generator, a MOSFET driver circuit, a load resistor, a turbine motor, the stabilization platform object, an attitude measurement circuit, a digital-to-analog converter, and an attitude calculation module, as shown in Figure 3.

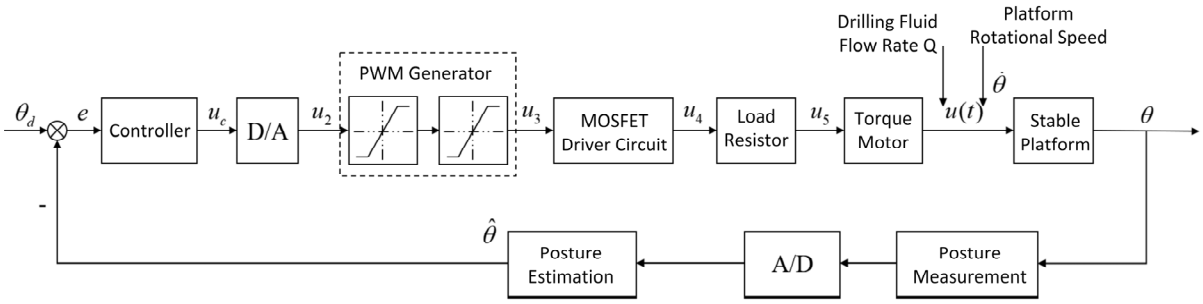

Figure 3. Block Diagram of the Angle Control System for the Tool Surface of the Stabilization Platform

Let the ideal value of the tool face angle be θ_d, and the calculated value be $\hat{\theta}$. Define the difference between the ideal value and the calculated value as e:

$$e = \theta_d - \hat{\theta} \tag{6}$$

Assume the controller's control law is:

$$u_c(t) = f(e,t) \tag{7}$$

Ignore the time delays and errors associated with components such as A/D and D/A converters, MOSFET driver circuits, and measurement sensors. Simplified as: $u_2(t) = u_c(t), u_4(t) = u_3(t), \hat{\theta} = \theta, \dot{\hat{\theta}} = \dot{\theta}$.

A PWM generator can be simply regarded as an amplification stage, described as:

$$u_3(t) = K_s \cdot u_2(t) \tag{8}$$

Through the MOSFET driver circuit, based on the function of the PWM pulse to turn the load resistor on and off, we have:

$$R(t) = u_5(t) = \frac{R_0}{u_4(t)} \tag{9}$$

Where R_0 represents the resistance value of the load resistor. In engineering applications, the load resistor's value is interchangeable, with a variation range of 5 to 30.

Based on the preceding analysis, the electromagnetic torque of the torque motor serves as the control driving torque for stabilizing the platform, denoted as $u(t) = T(t)$. Substituting this into the electromagnetic torque formula for AC motors, $u(t) = C_e \cdot \phi \cdot I(t) \cdot \cos\varphi$, yields:

$$u(t) = \frac{K_B k_T Q_{f\min}(1 + K_b |\cos \omega_B t|)}{R_0} \cdot u_3(t) - \frac{K_B \dot{\theta}}{R_0} \cdot u_3(t) \tag{10}$$

The flow rate-torque characteristic coefficient $K_q = \frac{K_B k_T}{R_0}$, the rotational speed-torque characteristic $K_\omega = \frac{K_B}{R_0}$, and the drilling fluid flow rate $Q(t) = Q_{f\min}(1 + K_b |\cos \omega_B t|)$ yield:

$$u(t) = K_q Q(t) \cdot u_3(t) - K_\omega \cdot \dot{\theta} \cdot u_3(t) \tag{11}$$

ISSN: 2688-8645

2.3. Stable Platform Dynamics Model Considering Sensor and Actuator Failure

Based on the above analysis, the flow rate change can be considered as an independent variable as $\dot{\theta}$ function $f(\dot{\theta}) = K_q Q - K_\omega \dot{\theta}$, which is regarded as an unknown control gain function and approximated using a fuzzy logic system, thus eliminating the effect of the flow rate change. Defining the state variable $x = [x_1, x_2] = [\theta, \omega]$ allows the stabilized platform control system model (5) to be simplified and include the form of transmission sensor and actuator faults

$$\begin{cases} \dot{x}_1 = x_2 \\ \dot{x}_2 = f(x) + g(x)v(t) + d(t) \\ y^f = \mu x_1 \end{cases} \tag{12}$$

where $f(x) = -\frac{k_1 x_2}{J} - \frac{f \sin x_1}{J}$ is the unknown smooth nonlinear function, is the unknown control gain function, and $d(t) = \frac{\Delta(t) + M_0}{J}$ is the uncertain perturbation signal. y^f represents the sensor failure fault, μ represents the fault parameter, and $v(t)$ represents the actuator fault.

(1) Sensor failure model

It is assumed that the sensor used to measure the system variable $\xi^f(t) \in R$ fails at moment T_f, as represented below [12]

$$\xi^f(t) = \mu\xi(t), 0 < \mu < 1 \quad \forall t > T_f \tag{13}$$

where $\xi^f(t)$ is the actual measured value of the sensor output and $0 < \mu < 1$ is the failure parameter. This case indicates a partial failure and according to the above definition, the measured output in the nonlinear system (5) in the presence of a sensor failure can be expressed as

$$y^f(t) = \begin{cases} y(t), & t \le T_f \\ \mu y(t), & t > T_f \end{cases} \tag{14}$$

Let $l = 1/\mu$, $\hat{l}$ be an estimate of l. Define the estimation error as $\tilde{l} = l - \hat{l}$.

(2) Actuator failure model

The two fault models for stabilized platform actuator failure are:

Failure model: $v(t) = \beta u(t)$

Bias fault model: $v(t) = \beta u(t) v(t) = u(t) + \bar{u}$

Therefore, the fault model that considers both failure and bias is

$$v(t) = \beta u(t) + \bar{u} \tag{15}$$

where β, u and $\bar{u}$ represent known constants, control input signals and unknown bounded functions respectively, then $\bar{u}$ satisfies $|\bar{u}| \le \omega_1$. Here ω_1 is an unknown constant.

Assumption 1: The unknown disturbance $d(t)$ is bounded, and there exists an unknown positive constant d^* such that $|d(t)| \le d^*$.

Assumption 2: For any moment of $t \ge 0$, the desired signal y_d and the first order derivative $\dot{y}_d$ are bounded.

ISSN: 2688-8645

Assumption 3 [13]: There exist positive constants g_1 and g_d such that $0 \le g_1 \le |g(x)| \le g_d$ holds.

Lemma 1 [14]: For a system $\dot{x} = f(x)$, if there exists a positive definite and continuous function $V(x)$ such that

$$\dot{V}(x) \le -cV^{\alpha}(x) + \psi \tag{16}$$

where $c > 0$, $\psi > 0$, and $0 < \alpha < 1$, then system $\dot{x} = f(x)$ is semi-globally practically finite time stable and the stabilization time is satisfied as

$$T_t \le \frac{V^{1-\alpha}(x_0)}{k\theta_0(1-\alpha)} \tag{17}$$

where $k > 0$, $0 < \theta_0 < 1$.

Lemma 2[15]: There exist real variables ϑ, ζ and positive constants ρ, κ and τ for which the following inequality holds:

$$|\vartheta|^{\rho}|\zeta|^{\kappa} \le \frac{\rho}{\rho+\kappa}\tau|\vartheta|^{\rho+\kappa} + \frac{\kappa}{\rho+\kappa}\tau^{\frac{-\rho}{\kappa}}|\zeta|^{\rho+\kappa} \tag{18}$$

Lemma 3[16]: A fuzzy logic system is a universal approximator that can approximate any unknown smooth nonlinear function. The fuzzy IF-THEN rule is expressed as follows

R^l: If x_1 is F_1^l, x_2 is F_2^l, ..., x_n is F_n^l, then y is G^l, $l = 1, 2, \cdots, N$.

where $x=[x_1,x_2,\cdots,x_n]^T$ and $x=[x_1,x_2,\cdots,x_n]^T$ are the inputs and outputs of the fuzzy logic system, respectively. The fuzzy affiliation functions $\mu_{F_i^l}(x_i)$ and $\mu_{G^l}(y)$ correspond to the fuzzy sets F_i^l and G^l respectively; N is the number of fuzzy rules.

The fuzzy logic system can be expressed as

$$y(x) = \frac{\sum_{l=1}^{N}\overline{y}_l\prod_{i=1}^{n}\mu_{F_i^l}(x_i)}{\sum_{l=1}^{N}\prod_{i=1}^{n}\mu_{F_i^l}(x_i)} \tag{19}$$

where $\overline{y}_l = \max_{y\in V}\mu_{G^l}(y)$.

The fuzzy basis function is defined as

$$\varphi_l = \frac{\prod_{i=1}^{n}\mu_{F_i^l}(x_i)}{\sum_{l=1}^{N}\prod_{i=1}^{n}\mu_{F_i^l}(x_i)} \tag{20}$$

where $\varphi(x) = [\varphi_1(x),\ \varphi_2(x),\ \ldots,\ \varphi_N(x)]^T$ is the fuzzy basis function vector and $\theta = [\theta_1,\ \theta_2,\ \ldots,\ \theta_N]^T$ is the adaptive parameter vector. Therefore, the output of the fuzzy logic system can be written as

$$y(x) = \theta^{\mathrm{T}}\varphi(x) \tag{21}$$

Let $f(x)$ be a continuous function defined in the closed set Ω. For any given positive constant ε, there exists a fuzzy logic system such that the following inequality holds

$$\sup_{x\in\Omega}|f(x) - \theta^{\mathrm{T}}\varphi(x)|,,\ \varepsilon \tag{22}$$

ISSN: 2688-8645

3. Fuzzy State Observer Design

To facilitate the design of the state observer, system (14) is rewritten in the following form

$$\begin{cases} \dot{x} = Ax + Ky + B\left[f(x) + d\right] + Bg(x)(\beta u + \bar{u}) \\ y^f = \mu C^T x \end{cases} \tag{23}$$

where $x = [x_1, x_2]^T$ is the system state vector, $A = \begin{bmatrix} -k_1 & 1 \\ -k_2 & 0 \end{bmatrix}, B = \begin{bmatrix} 1 \\ 0 \end{bmatrix}, K = \begin{bmatrix} k_1 \\ k_2 \end{bmatrix}, C = \begin{bmatrix} 1 \\ 0 \end{bmatrix}$

Based on the measured output signal y^f and Eq. (25), then the form of the state observer is constructed as follows

$$\begin{cases} \dot{\hat{x}} = A\hat{x} + K\hat{l}y^f + B\hat{f}(\hat{x} \mid \hat{\theta}) + B\hat{g}(\hat{x} \mid \hat{\theta}_g)\beta u \\ \hat{y} = C^T\hat{x} \end{cases} \tag{24}$$

where $\hat{x}_1$ and $\hat{x}_2$ are the state observations of x_1 and x_2 respectively, k_1 and k_2 are the observer gain vectors and $\hat{l}$ is the estimate of l.

Using fuzzy logic system $\hat{f}(x \mid \hat{\theta}) = \hat{\theta}^T\varphi(x)$ approximates $f(x)$, $\hat{g}(x \mid \hat{\theta}_g) = \hat{\theta}^T\varphi_g(x)$ approximates $g(x)$. Assumptions

$$f(x) = \theta^{*T}\varphi(x) + \varepsilon \tag{25}$$

$$g(x) = \theta_g^{*T}\varphi_g(x) + \varepsilon_g \tag{26}$$

where θ^* and θ_g^* are optimal parameters; ε and ε_g are bounded fuzzy approximation errors. Assume that there exist positive constants ε^* and ε_g^* satisfying $\|\varepsilon\| \le \varepsilon^*$ and $\|\varepsilon_g\| \le \varepsilon_g^*$.

Define the observation error as $\tilde{x} = x - \hat{x}$. Combining Eq. (16) and (17), the derivation is obtained

$$\begin{aligned} \dot{\tilde{x}} &= \dot{x} - \dot{\hat{x}} \\ &= A\tilde{x} + B\delta + B\delta_g u + BK\tilde{l}y^f + Bd \\ &\quad + Bg(x)\bar{u} \end{aligned} \tag{27}$$

where $\delta = f(x) - \hat{f}(\hat{x} \mid \theta_g), \delta_g = g(x) - \hat{g}(\hat{x} \mid \hat{\theta}_g)$.

It follows from the definitions of δ and δ_g

$$\delta = \theta^{*T}(\varphi(x) - \varphi(\hat{x})) + \tilde{\theta}\varphi(\hat{x}) + \varepsilon \tag{28}$$

$$\delta_g = \theta_g^{*T}(\varphi_g(x) - \varphi_g(\hat{x})) + \tilde{\theta}_g^T\varphi_g(\hat{x}) + \varepsilon_g \tag{29}$$

Choosing the appropriate k_1 and k_2 ensures that A is a strictly Hurwitz matrix. Therefore, there exist positive definite matrices $Q = Q^T$, $P = P^T$, with the following relations holding:

$$A^TP + PA = -2Q \tag{30}$$

The following Lyapunov function is considered to evaluate the properties of the designed fuzzy state observer.

$$V_0 = \frac{1}{2}\tilde{x}^TP\tilde{x} \tag{31}$$

Seek guidance, there

ISSN: 2688-8645

$$\begin{aligned}\dot{V}_0 &= \frac{1}{2}\dot{\tilde{x}}^T P\tilde{x} + \frac{1}{2}\tilde{x}^T P\dot{\tilde{x}} \\ &= \frac{1}{2}\tilde{x}^T[A^T P + PA]\tilde{x} + \tilde{x}^T PB(\delta + \delta_g u + d + K\tilde{l}y^f + g(x)\bar{u}) \\ &= -\tilde{x}^T Q\tilde{x} + \tilde{x}^T PB\delta + \tilde{x}^T PB\delta_g u + \tilde{x}^T PBd + \tilde{x}^T PBK\tilde{l}y^f + \tilde{x}^T PBg(x)\bar{u} \\ &= -\tilde{x}^T Q\tilde{x} + \tilde{x}^T PB\varepsilon + \tilde{x}^T PB\varepsilon_g u + \tilde{x}^T PBd + \tilde{x}^T PBK\tilde{l}y^f + \tilde{x}^T PB\theta^{*T}(\varphi(x) - \varphi(\hat{x})) \\ &\quad + \tilde{x}^T PB\tilde{\theta}\varphi(\hat{x}) + \tilde{x}^T PB\theta_g^{*T}(\varphi_g(x) - \varphi_g(\hat{x}))u + \tilde{x}^T PB\tilde{\theta}_g^T\varphi_g(\hat{x})u + \tilde{x}^T PBg(x)\bar{u}\end{aligned} \tag{32}$$

According to Young's inequality and $0 < \varphi_i^T(\cdot)\varphi_i(\cdot) \le 1$, it can be obtained

$$\begin{aligned}\tilde{x}^T PB\varepsilon + \tilde{x}^T PB\varepsilon_g u + \tilde{x}^T PBd + \tilde{x}^T PBK\tilde{l}y^f \le{}& 2\|\tilde{x}\|^2 + \frac{1}{2}\|P\|^2\varepsilon^{*2} \\ &+ \frac{1}{2}\|P\|^2\varepsilon_g^{*2}u^2 + \frac{1}{2}\|P\|^2 d^{*2} \\ &+ \frac{1}{2}\|P\|^2(k_1^2 + k_2^2)(\tilde{l}y^f)^2\end{aligned} \tag{33}$$

$$\tilde{x}^T PB\tilde{\theta}^T\varphi(\hat{x}) \le \frac{1}{2}\|\tilde{x}\|^2 + \frac{1}{2}\|P\|^2\|\theta\|^2 \tag{34}$$

$$\tilde{x}^T PBg(x)\bar{u} \le \frac{1}{2}\|\tilde{x}\|^2 + \frac{1}{2}\|P\|^2 g_d{}^2\omega_1{}^2 \tag{35}$$

$$\tilde{x}^T PB\theta^{*T}(\varphi(x) - \varphi(\hat{x})) \le \|\tilde{x}\|^2 + \|P\|^2\|\theta^*\|^2 \tag{36}$$

$$\tilde{x}^T PB\tilde{\theta}_g^T\varphi_g(\hat{x})u \le \frac{1}{2}\|\tilde{x}\|^2 + \frac{1}{2}\|P\|^2\|\tilde{\theta}_g\|^2 u^2 \tag{37}$$

$$\tilde{x}^T PB\theta_g^{*T}(\varphi(x) - \varphi(\hat{x}))u \le \|\tilde{x}\|^2 + \|P\|^2\|\theta_g^*\|^2 u^2 \tag{38}$$

Substituting equation (33) to equation (38) into equation (32), it can be obtained

$$\begin{aligned}\dot{V}_0 &\le -\tilde{x}^T Q\tilde{x} + \frac{11}{2}\|\tilde{x}\|^2 + \|P\|^2(\frac{1}{2}\varepsilon^{*2} + \frac{1}{2}d^{*2} + \frac{1}{2}g_d{}^2\omega_1{}^2 + \|\theta^*\|^2) + \frac{1}{2}\|P\|^2\varepsilon_g^{*2}u^2 \\ &\quad + \frac{1}{2}\|P\|^2\|\tilde{\theta}\|^2 + \frac{1}{2}\|P\|^2\|\tilde{\theta}_g\|^2 u^2 + \|P\|^2\|\theta_g^*\|^2 u^2 + \frac{1}{2}\|P\|^2(k_1^2 + k_2^2)(\tilde{l}y^f)^2 \\ &\le -\lambda_0\|\tilde{x}\|^2 + \frac{1}{2}\|P\|^2\|\tilde{\theta}\|^2 + (\frac{1}{2}\|P\|^2\|\tilde{\theta}_g\|^2 + \rho_0)u^2 + \frac{1}{2}\|P\|^2(k_1^2 + k_2^2)(\tilde{l}y^f)^2 + D_0\end{aligned} \tag{39}$$

where $\lambda_0 = \lambda_{\min}(Q) - \frac{11}{2}$, $D_0 = \|P\|^2(\frac{1}{2}\varepsilon^{*2} + \frac{1}{2}d^{*2} + \frac{1}{2}g_d{}^2\omega_1{}^2 + \|\theta^*\|^2)$, $\rho_0 = \|P\|^2\|\theta_g^*\|^2 + \frac{1}{2}\|P\|^2\varepsilon_g^{*2}$.

4. Controller Design and Stability Analysis

4.1. Controller Design

In this section, the dynamic surface control technique is used to solve the 'computational explosion' problem in the traditional backstepping control technique by embedding the outputs obtained from the dynamic surfaces into the stability analysis and replacing the derivatives of the virtual controller. Firstly, the tracking error is defined as $z_1 = y - y_d$, the virtual error in the second step is defined as $z_2 = \hat{x}_2 - \beta_1$, and the virtual control law is defined as α_1.

ISSN: 2688-8645

Taking β_1 to be the output of the low-pass filter $\frac{1}{\omega s+1}$ of α_1 and satisfying $\begin{cases}\omega\dot{\beta}_1+\beta_1=\alpha_1\\ \beta_1(0)=\alpha_1(0)\end{cases}$, can be obtained

$$\dot{\beta}_1=\frac{\alpha_1-\beta_1}{\omega} \tag{40}$$

Define the filter error generated as

$$e_1=\beta_1-\alpha_1 \tag{41}$$

Since the occurrence time and value of sensor faults are uncertain, this means that both T_f and μ are unknown. Therefore, tracking the change in error z_1 is the main difficulty in output feedback tracking control. When a fault occurs, z_1 will undergo the following changes

$$z_1=y-y_d \xrightarrow{T_f} z_1=y^f/\mu-y_d$$

Due to the presence of sensor faults, the system output cannot be used for controller design. An algorithm needs to be designed to compensate for the effects of sensor faults. Therefore, the following error changes are designed

$$z_1=x_1-y_d=\hat{l}y-y_d+\tilde{l}y=\hat{z}_1+\tilde{l}y \tag{42}$$

where $\hat{z}_1=\hat{l}y-y_d$ is known.

Using the first-order filter introduced above, the following are the steps for stability analysis and controller design.

Step 1: For the first tracking error $z_1=y-y_d$, its derivative can be obtained as follows

$$\dot{z}_1=\dot{y}-\dot{y}_d=x_2-\dot{y}_d=\hat{x}_2+\tilde{x}_2-\dot{y}_d \tag{43}$$

Substituting the virtual error $z_2=\hat{x}_2-\beta_1$ from step 2 into equation (36), we obtain

$$\dot{z}_1=z_2+\alpha_1+e_1+\tilde{x}_2-\dot{y}_d \tag{44}$$

Design the following Lyapunov function

$$V_1=V_0+\frac{1}{2}z_1^2+\frac{1}{3\gamma_1}\left|\tilde{l}\right|^3+\frac{1}{2}e_1^2 \tag{45}$$

where $\gamma_1>0$ is the design parameter. Taking the derivative and substituting equation (45) yields

$$\begin{aligned}\dot{V}_1&=\dot{V}_0+z_1\dot{z}_1-\frac{1}{\gamma_1}\tilde{l}^2\dot{\hat{l}}\,\mathrm{sgn}(\tilde{l})+e_1\dot{e}_1\\&=\dot{V}_0+e_1\dot{e}_1+z_1(z_2+\alpha_1+e_1+\tilde{x}_2-\dot{y}_d)-\frac{1}{\gamma_1}\tilde{l}^2\dot{\hat{l}}\,\mathrm{sgn}(\tilde{l})\\&\le-\lambda_0\left\|\tilde{x}\right\|^2+\frac{1}{2}\left\|P\right\|^2\left\|\tilde{\theta}\right\|^2+(\frac{1}{2}\left\|P\right\|^2\left\|\tilde{\theta}_g\right\|^2+\rho_0)u^2+\frac{1}{2}\left\|P\right\|^2(k_1^2+k_2^2)(\tilde{l}y^f)^2\\&\quad+D_0+e_1\dot{e}_1+z_1(z_2+\alpha_1+e_1+\tilde{x}_2-\dot{y}_d)-\frac{1}{\gamma_1}\tilde{l}^2\dot{\hat{l}}\,\mathrm{sgn}(\tilde{l})\end{aligned} \tag{46}$$

According to Young's inequality, the following inequality can be obtained

$$z_1\tilde{x}_2+z_1e_1\le z_1^2+\frac{1}{2}\left\|\tilde{x}\right\|^2+\frac{1}{2}e_1^2 \tag{47}$$

Substituting equation (47) into equation (48) yields

ISSN: 2688-8645

$$\begin{aligned}\dot{V}_1 \le & -\lambda_1 \|\tilde{x}\|^2 + \frac{1}{2}\|P\|^2 \|\tilde{\theta}\|^2 + (\frac{1}{2}\|P\|^2 \|\tilde{\theta}_g\|^2 + \rho_0)u^2 + \frac{1}{2}\|P\|^2 (k_1^2 + k_2^2)(\tilde{l}y^f)^2 + D_0 \\ & + e_1\dot{e}_1 + z_1(\alpha_1 - \dot{y}_d) + z_1 z_2 + z_1^2 + \frac{1}{2}e_1^2 - \frac{1}{\gamma_1}\tilde{l}^2\dot{\hat{l}}\,\mathrm{sgn}(\tilde{l})\end{aligned} \tag{48}$$

where $\lambda_1 = \lambda_0 - \frac{1}{2}$.

Design virtual control law A as follows:

$$\alpha_1 = -c_1\hat{z}_1^{2y-1} + \dot{y}_d \tag{49}$$

where $c_1 > 3/2$ is the design parameter.

Substituting (49) into (48), we obtain:

$$\begin{aligned}\dot{V}_1 \le & -\lambda_1 \|\tilde{x}\|^2 + \frac{1}{2}\|P\|^2 \|\tilde{\theta}\|^2 + (\frac{1}{2}\|P\|^2 \|\tilde{\theta}_g\|^2 + \rho_0)u^2 \\ & + \frac{1}{2}\|P\|^2 (k_1^2 + k_2^2)(\tilde{l}y^f)^2 + e_1\dot{e}_1 - c_1 z_1 \hat{z}_1^{2y-1} + z_1 z_2 \\ & + \frac{3}{2}z_1^2 + \frac{1}{2}e_1^2 - \frac{1}{\gamma_1}\tilde{l}^2\dot{\hat{l}}\,\mathrm{sgn}(\tilde{l}) + D_0\end{aligned} \tag{50}$$

According to Young's inequality, we obtain

$$\begin{aligned}-c_1 z_1 \hat{z}_1 &= -c_1 z_1 (z_1 - \tilde{l}y^f) \\ &\le -c_1 z_1^2 + \xi(c_1 \tilde{l}y^f \hat{z}_1)^{2y-1} + \frac{1}{4\xi} + c_1(\tilde{l}y^f)^2\end{aligned} \tag{51}$$

Among them, ξ is a design parameter that will play an important role in the design of the adaptive law. Its selection and its impact on the estimation of the failure coefficient will be given in the subsequent design.

Substituting equation (51) into equation (50), we obtain

$$\begin{aligned}\dot{V}_1 \le & -\lambda_1 \|\tilde{x}\|^2 + \frac{1}{2}\|P\|^2 \|\tilde{\theta}\|^2 + (\frac{1}{2}\|P\|^2 \|\tilde{\theta}_g\|^2 + \rho_0)u^2 + \frac{1}{2}\|P\|^2 (k_1^2 + k_2^2)(\tilde{l}y^f)^2 + D_0 + e_1\dot{e}_1 \\ & -C_1 z_1^2 + \xi(c_1 \tilde{l}y^f \hat{z}_1)^2 + \frac{1}{4\xi} + c_1(\tilde{l}y^f)^2 + z_1 z_2 + \frac{1}{2}e_1^2 - \frac{1}{\gamma_1}\tilde{l}^2\dot{\hat{l}}\,\mathrm{sgn}(\tilde{l})\end{aligned} \tag{52}$$

where $C_1 = c_1 - 3/2 > 0$ is the design parameter.

Design adaptive parameters

$$\dot{\hat{l}} = \begin{cases}\gamma_1(\xi c_1^2 \hat{z}_1^2 + c_1 + \frac{1}{2}\|P\|^2 (k_1^2 + k_2^2))(y^f)^2 - \sigma_1 \hat{l}, & m > 0 \\ 0, & m \le 0\end{cases} \tag{53}$$

where $m = \gamma_1(\xi c_1^2 \hat{z}_1^{2y-1} + c_1 + \frac{1}{2}\|P\|^2 (k_1 + k_2))(y^f)^2$ and σ_1 are design parameters.

Note: From equation (42), it can be seen that z_1 will change rapidly due to sensor failure. According to equation (53), ξ can be designed to compensate for sensor failure. In order to improve the sensitivity of ξ to changes in z_1, ξ should be selected to be large enough. At the same time, in order to reduce the impact of other items in equation (46) on the adaptive law, γ_1 should be selected to be small enough.

Substituting (53) into (52) yields

ISSN: 2688-8645

$$\begin{aligned}\dot{V}_1 \le & -\lambda_1\|\tilde{x}\|^2+\frac{1}{2}\|P\|^2\|\tilde{\theta}\|^2+(\frac{1}{2}\|P\|^2\|\tilde{\theta}_g\|^2+\rho_0)(x_3-u)^2\\ & +D_1+e_1\dot{e}_1-C_1z_1^2+z_1z_2+\frac{1}{2}e_1^{\,2}+\frac{\sigma_1}{\gamma_1}\tilde{l}^2\hat{l}\,\mathrm{sgn}(\tilde{l})\end{aligned} \tag{54}$$

where $D_1=D_0+\frac{1}{4\xi}$.

Step 2: The virtual error in the second step is defined as $z_2=\hat{x}_2-\beta_1$. Differentiation yields

$$\begin{aligned}\dot{z}_2 &= \dot{\hat{x}}_2-\dot{\beta}_1\\ &= \hat{g}(\hat{x})\beta u+\hat{f}(\hat{x})+k_2(\hat{l}y^f-\hat{x}_1)-\dot{\beta}_1\end{aligned} \tag{55}$$

Design the following Lyapunov function

$$V_2=V_1+\frac{1}{2}z_2^2+\frac{1}{2\gamma_2}\tilde{\theta}^T\tilde{\theta}+\frac{1}{2\gamma_3}\tilde{\theta}_g^T\tilde{\theta}_g \tag{56}$$

where $\gamma_2>0$ and $\gamma_3>0$ are design parameters. Differentiation yields

$$\begin{aligned}\dot{V}_2 &= \dot{V}_1+z_2\dot{z}_2+\frac{1}{\gamma_2}\tilde{\theta}^T\dot{\tilde{\theta}}+\frac{1}{\gamma_3}\tilde{\theta}_g^T\dot{\tilde{\theta}}_g\\ &\le -\lambda_1\|\tilde{x}\|^2+\frac{1}{2}\|P\|^2\|\tilde{\theta}\|^2+(\frac{1}{2}\|P\|^2\|\tilde{\theta}_g\|^2+\rho_0)u^2+D_1+e_1\dot{e}_1-C_1z_1^2+\frac{1}{2}e_1^{\,2}+z_1z_2\\ &+z_2(\hat{\theta}_g^T\varphi_g(\hat{x})\beta u+\hat{\theta}^T\varphi(\hat{x})+k_2(\hat{l}y^f-\hat{x}_1)-\dot{\beta}_1)-z_2\tilde{\theta}_g^T\varphi_g(\hat{x})u-z_2\tilde{\theta}^T\varphi(\hat{x})\\ &+\frac{\sigma_1}{\gamma_1}\tilde{l}^2\hat{l}\,\mathrm{sgn}(\tilde{l})+\frac{1}{\gamma_2}\tilde{\theta}^{\mathrm{T}}(\gamma_2z_2\varphi(\hat{x})-\dot{\hat{\theta}})+\frac{1}{\gamma_3}\tilde{\theta}_g^T(\gamma_2z_2\varphi_g(\hat{x})u-\dot{\hat{\theta}}_g)\end{aligned} \tag{57}$$

According to Young's inequality, the following inequality can be obtained

$$-z_2\tilde{\theta}_g^T\varphi_g(\hat{x})u\le\frac{1}{2}z_2^2+\frac{1}{2}\|\tilde{\theta}_g\|^2u^2 \tag{58}$$

$$-z_2\tilde{\theta}^T\varphi(\hat{x})\le\frac{1}{2}z_2^2+\frac{1}{2}\|\tilde{\theta}\|^2 \tag{59}$$

Substituting (58) and (59) into (57), we obtain

$$\begin{aligned}\dot{V}_2 \le & -\lambda_1\|\tilde{x}\|^2+\frac{1}{2}\|P\|^2\|\tilde{\theta}\|^2+(\frac{1}{2}\|P\|^2\|\tilde{\theta}_g\|^2+\rho_0)u^2+D_1+e_1\dot{e}_1-C_1z_1^2+\frac{1}{2}e_1^{\,2}+z_1z_2\\ &+z_2(\hat{\theta}_g^T\varphi_g(\hat{x})\beta u+\hat{\theta}^T\varphi(\hat{x})+k_2(\hat{l}y^f-\hat{x}_1)-\dot{\beta}_1)+z_2^2+\frac{1}{2}\|\tilde{\theta}_g\|^2u^2+\frac{1}{2}\|\tilde{\theta}\|^2\\ &+\frac{\sigma_1}{\gamma_1}\tilde{l}^2\hat{l}\,\mathrm{sgn}(\tilde{l})+\frac{1}{\gamma_2}\tilde{\theta}^{\mathrm{T}}(\gamma_2z_2\varphi(\hat{x})-\dot{\hat{\theta}})+\frac{1}{\gamma_3}\tilde{\theta}_g^T(\gamma_3z_2\varphi_g(\hat{x})u-\dot{\hat{\theta}}_g)\end{aligned} \tag{60}$$

The adaptive law for design control input u and parameters $\hat{\theta}$ and $\hat{\theta}_g$ is as follows

$$u=[\beta\hat{\theta}_g^T\varphi_g(\hat{x})]^{-1}(-c_2z_2^{\,2\gamma-1}-z_2-z_1-\hat{\theta}^T\varphi(\hat{x})-k_2(\hat{l}y^f-\hat{x}_1)+\frac{\alpha_1\text{-}\beta_1}{\omega}) \tag{61}$$

$$\dot{\hat{\theta}}=\gamma_2z_2\varphi(\hat{x})-\sigma_2\hat{\theta} \tag{62}$$

$$\dot{\hat{\theta}}_g=\gamma_3z_2\varphi_g(\hat{x})u-\sigma_3\hat{\theta}_g \tag{63}$$

where $c_2>0$, $0<\gamma<1$, $\sigma_2>0$, and $\sigma_3>0$ are design parameters.

Substituting equations (61), (62), and (63) into (60) yields

ISSN: 2688-8645

$$\dot{V}_2 \le -\lambda_1 \|\tilde{x}\|^2 + \frac{1}{2}\|P\|^2 \|\tilde{\theta}\|^2 + (\frac{1}{2}(\|P\|^2 (\tilde{\theta}_g)^2 + \rho_0)u^2 + D_1 + e_1\dot{e}_1 - C_1 z_1^2 + \frac{1}{2}e_1^2$$
$$- c_2 z_2^{2\gamma} + \frac{1}{2}\|\tilde{\theta}_g\|^2 u^2 + \frac{1}{2}\|\tilde{\theta}\|^2 + \frac{\sigma_1}{\gamma_1}\tilde{l}^2\hat{l}\,\mathrm{sgn}(\tilde{l}) + \frac{\sigma_2}{\gamma_2}\tilde{\theta}^{\mathrm{T}}\hat{\theta} + \frac{\sigma_3}{\gamma_3}\tilde{\theta}_g^T\hat{\theta}_g \quad (64)$$

4.2. Stability Analysis

To ensure the stability of the entire system, the Lyapunov function selected based on the aforementioned analysis is

$$V = \frac{1}{2}\tilde{x}^T P\tilde{x} + \frac{1}{2}e_1^2 + \frac{1}{2}z_1^2 + \frac{1}{3\gamma_1}|\tilde{l}|^3 + \frac{1}{2}z_2^2 + \frac{1}{2\gamma_2}\tilde{\theta}^T\tilde{\theta} + \frac{1}{2\gamma_3}\tilde{\theta}_g^T\tilde{\theta}_g \quad (65)$$

Differentiation yields

$$\dot{V}_2 \le -\lambda_1 \|\tilde{x}\|^2 + \frac{1}{2}\|P\|^2 \|\tilde{\theta}\|^2 + (\frac{1}{2}(\|P\|^2 (\tilde{\theta}_g)^2 + \rho_0)u^2 + D_1 + e_1\dot{e}_1 - C_1 z_1^2 + \frac{1}{2}e_1^2$$
$$- c_2 z_2^{2\gamma} + \frac{1}{2}\|\tilde{\theta}_g\|^2 u^2 + \frac{1}{2}\|\tilde{\theta}\|^2 + \frac{\sigma_1}{\gamma_1}\tilde{l}^2\hat{l}\,\mathrm{sgn}(\tilde{l}) + \frac{\sigma_2}{\gamma_2}\tilde{\theta}^{\mathrm{T}}\hat{\theta} + \frac{\sigma_3}{\gamma_3}\tilde{\theta}_g^T\hat{\theta}_g \quad (66)$$

From (53), we can see that $\dot{\hat{l}} \ge 0$, $\lim_{t\to\infty}\hat{l}(t) = l$, therefore $l > \hat{l}$. Again, because $\tilde{l} = l - \hat{l}$, therefore $\tilde{l} > 0$.

By Young's inequality, the following inequality can be obtained

$$\tilde{l}^2\hat{l}\,\mathrm{sgn}(\tilde{l}) = \tilde{l}^2(l_1 - \tilde{l}_1) \le \frac{1}{3}l^3 - \frac{1}{3}|\tilde{l}|^3 \quad (67)$$

$$\tilde{\theta}^T\hat{\theta} = \tilde{\theta}^T(\theta^* - \tilde{\theta}) \le -\frac{1}{2}\|\tilde{\theta}\|^2 + \frac{1}{2}\|\theta^*\|^2 \quad (68)$$

$$\tilde{\theta}_g^T\hat{\theta}_g = \tilde{\theta}_g^T(\theta_g^* - \tilde{\theta}_g) \le -\frac{1}{2}\|\tilde{\theta}_g\|^2 + \frac{1}{2}\|\theta_g^*\|^2 \quad (69)$$

Substituting (60), (61), and (62) into (59) yields

$$\dot{V} \le -\lambda_1 \|\tilde{x}\|^2 + (\frac{1}{2}\|P\|^2 - \frac{\sigma_2}{2\gamma_2} + \frac{1}{2})\|\tilde{\theta}\|^2 + e_1\dot{e}_1 - C_1 z_1^2 - c_2 z_2^{2\gamma} + \frac{1}{2}e_1^2$$
$$- \frac{\sigma_1}{3\gamma_1}|\tilde{l}|^3 - \frac{\sigma_3}{2\gamma_3}\|\tilde{\theta}_g\|^2 + D_2 \quad (70)$$

where $D_2 = D_1 + \frac{\sigma_1}{3\gamma_1}l^3 + \frac{\sigma_2}{2\gamma_2}\|\theta^*\|^2 + \frac{\sigma_3}{2\gamma_3}\|\theta_g^*\|^2 + (\frac{1}{2}(\|P\|^2 (\tilde{\theta}_g)^2 + \rho_0)(x_3 - u)^2 + \frac{1}{2}\|\tilde{\theta}_g\|^2 u^2$.

Through equation (41), we can obtain its derivative as

$$\dot{e}_1 = \dot{\beta}_1 - \dot{\alpha}_1 = -\frac{e_1}{\omega} + B_1(\cdot) \quad (71)$$

According to reference [15], it can be seen that $B_1(\cdot)$ in equation (64) is a continuous and bounded function, and satisfies relation $B_1(\cdot) = B_1(z_1, e_1, y_d, \dot{y}_d, \ddot{y}_d) = -\dot{\alpha}_1 = c_1\dot{\tilde{z}}_1 - \ddot{y}_d$.

In dynamic surface control, the introduction of a first-order filter avoids the “computational explosion” caused by repeated differentiation of the virtual control law. However, this introduces new filter error. By performing bounded scaling on the filter error, we ensure that the filter error does not compromise the closed-loop stability of the system. It is demonstrated that its impact is finite and can be suppressed by control parameters.

From Young's inequality, we obtain

ISSN: 2688-8645

$$e_1\dot{e}_1 \le -\frac{e_1^{\,2}}{\omega} + \left|e_1 B_1(\cdot)\right| \le -\frac{e_1^{\,2}}{\omega} + \frac{1}{2}e_1^{\,2} + \frac{1}{2}M^2 \tag{72}$$

where M is the maximum value of $B_1(\cdot)$.

Equation (73) can be further derived as follows

$$\begin{aligned}\dot{V} \le & -\lambda_1\left\|\tilde{x}\right\|^2 - (\frac{\sigma_2}{2\gamma_2} - \frac{1}{2} - \frac{1}{2}\left\|P\right\|^2)\left\|\tilde{\theta}\right\|^2 - (\frac{1}{\omega} - 1)e_1^{\,2} - C_1 z_1^2 - c_2 z_2^{2\gamma} \\ & - \frac{\sigma_1}{3\gamma_1}|\tilde{l}\,|^3 - \frac{\sigma_3}{2\gamma_3}\left\|\tilde{\theta}_g\right\|^2 + H\end{aligned} \tag{73}$$

where $H = D_2 + \frac{1}{2}M^2$.

Theorem 1: For nonlinear systems (12), considering sensor faults and actuator faults, given the initial state and reference signal of the system, the system achieves semi-global actual finite-time stability through the constructed intermediate variable function (58), actual controller (61), and adaptive parameter update laws (62) and (63). With appropriate parameter adjustments, the convergence residual can converge to a small residual set close to zero.

Proof: First, rewrite equation (73) as

$$\begin{aligned}\dot{V} \le & -\lambda_1\left\|\tilde{x}\right\|^2 - (\lambda_1\left\|\tilde{x}\right\|^2)^\gamma + (\lambda_1\left\|\tilde{x}\right\|^2)^\gamma - (\frac{\sigma_2}{2\gamma_2} - \frac{1}{2} - \frac{1}{2}\left\|P\right\|^2)\left\|\tilde{\theta}\right\|^2 \\ & - ((\frac{\sigma_2}{2\gamma_2} - \frac{1}{2} - \frac{1}{2}\left\|P\right\|^2)\left\|\tilde{\theta}\right\|^2)^\gamma + ((\frac{\sigma_2}{2\gamma_2} - \frac{1}{2} - \frac{1}{2}\left\|P\right\|^2)\left\|\tilde{\theta}\right\|^2)^\gamma - (\frac{1}{\omega} - 1)e_1^{\,2} \\ & - ((\frac{1}{\omega} - 1)e_1^{\,2})^\gamma + ((\frac{1}{\omega} - 1)e_1^{\,2})^\gamma - C_1 z_1^2 - (-C_1 z_1^2)^\gamma + (-C_1 z_1^2)^\gamma - c_2 z_2^{2\gamma} \\ & - \frac{\sigma_1}{3\gamma_1}|\tilde{l}\,|^3 - (\frac{\sigma_1}{3\gamma_1}|\tilde{l}\,|^3)^\gamma + (\frac{\sigma_1}{3\gamma_1}|\tilde{l}\,|^3)^\gamma - \frac{\sigma_3}{2\gamma_3}\left\|\tilde{\theta}_g\right\|^2 \\ & - (\frac{\sigma_3}{2\gamma_3}\left\|\tilde{\theta}_g\right\|^2)^\gamma + (\frac{\sigma_3}{2\gamma_3}\left\|\tilde{\theta}_g\right\|^2)^\gamma + H\end{aligned} \tag{74}$$

According to Lemma 2, define $\vartheta = \lambda_1\left\|\tilde{x}\right\|^2$, $(\frac{\sigma_2}{2\gamma_2} - \frac{1}{2} - \frac{1}{2}\left\|P\right\|^2)\left\|\tilde{\theta}\right\|^2$, $(\frac{1}{\omega} - 1)e_1^{\,2}$, $-C_1 z_1^2$, $\frac{\sigma_1}{3\gamma_1}|\tilde{l}\,|^3$, $\frac{\sigma_3}{2\gamma_3}\left\|\tilde{\theta}_g\right\|^2$, $\zeta = 1$, $\rho = \gamma$, $\kappa = 1-\gamma$, $\tau = \frac{1}{\gamma}$, $\pi = (1-\gamma)(\frac{1}{\gamma})^{\frac{\gamma}{\gamma-1}}$.

The result can be obtained

$$\begin{aligned}\dot{V} \le & -(\lambda_1\left\|\tilde{x}\right\|^2)^\gamma - ((\frac{\sigma_2}{2\gamma_2} - \frac{1}{2} - \frac{1}{2}\left\|P\right\|^2)\left\|\tilde{\theta}\right\|^2)^\gamma - ((\frac{1}{\omega} - 1)e_1^{\,2})^\gamma - (-C_1 z_1^2)^\gamma \\ & - c_2 z_2^{2\gamma} - (\frac{\sigma_1}{3\gamma_1}|\tilde{l}\,|^3)^\gamma - (\frac{\sigma_3}{2\gamma_3}\left\|\tilde{\theta}_g\right\|^2)^\gamma + C_2\end{aligned} \tag{75}$$

where $C_2 = H + 6\pi$.

According to equation (75), the following results can be obtained

$$\dot{V} \le -\Phi V_n^\gamma + C_2 \tag{76}$$

where $\Phi = \min\{(\frac{2(\lambda_{\min}(Q) - 11/2)}{\lambda_{\max}(P)})^\gamma, c_2 2^\gamma, (\frac{1}{\omega} - 1)^\gamma, \sigma_1^{\,\gamma}, (\frac{\sigma_2}{2\gamma_2} - \frac{1}{2} - \frac{1}{2}\left\|P\right\|^2)^\gamma, \sigma_3^{\,\gamma}$.

ISSN: 2688-8645

According to Lemma 3, it can be concluded that the controlled system is semi-globally actual finite-time bounded. Based on equation (69), it can be proven that the constructed state observer is bounded within a finite time, and the convergence error can converge to a small residual set near zero within a finite time. Even when both the sensors and actuators fail simultaneously, the system can still achieve finite-time convergence, and all signals in the controlled system are bounded within a finite time interval.

5. Simulation Results and Analysis

In this section, the effectiveness of the designed control algorithm is verified by simulation experiments. The stabilized platform model parameters: $J = 0.0285(kg \cdot m^2)$, $k_1 = 0.0008$, $f = 0.5$, $M_0 = -0.05$, $k_q = 1/12$, $k_\omega = 0.08/\pi$.

The disturbance torque acting on the platform is $\Delta(t) = \Delta_1(t) + \Delta_2(t) + \Delta_3(t)$. $\Delta_1(t)$ is a cosine disturbance form, which can be expressed as $\Delta_1(t) = \cos(3\pi t)$; $\Delta_2(t)$ can be simplified as a pair of pulses with frequency $\omega = 3Hz$, phase difference φ equal to 1/2 of a cycle, and amplitude $M_d = 0.46N \cdot m$; $\Delta_3(t)$ can be regarded as a zero-mean random disturbance, which can be expressed as $\Delta_3(t) = 0.5 \cdot rand(t)$.

Select the following membership functions for variables x_1 and x_2

$$\mu_{F_i^l}(\hat{x}_1) = \exp[-\frac{\left((\hat{x}_1 + 2 - (l-1)/2)^2\right)}{4}]$$

$$\mu_{F_i^l}(\hat{x}_2) = \exp[-\frac{\left((\hat{x}_2 + 2 - (l-1)/2)^2\right)}{4}]$$

where $l = 1,2,...,9$. The fuzzy basis function of the fuzzy system is

$$\varphi_{g,l}(\hat{x}_2) = \frac{\mu_{F_2^l}(\hat{x}_2)}{\sum_{l=1}^{9} \mu_{F_2^l}(\hat{x}_2)}$$

$$\varphi_{2,l}(\hat{x}_1, \hat{x}_2) = \frac{\mu_{F_1^l}(\hat{x}_1)\mu_{F_2^l}(\hat{x}_2)}{\sum_{l=1}^{9} \mu_{F_1^l}(\hat{x}_1)\mu_{F_2^l}(\hat{x}_2)}$$

The initial conditions for the system state are set to $x_1(0) = 0.1$, $x_2(0) = 0.1$, and the initial conditions for the observer are set to $\hat{x}_1(0) = 0$, $\hat{x}_2(0) = 0$. The initial values for the adaptive parameters are set to $\hat{l}(0) = 1$, $\hat{\theta}_g(0) = 0.1, \hat{\theta}(0) = 0.1$.

The design parameters are selected as follows: $c_1 = 2, c_2 = 6, \gamma_1 = 0.0001, \gamma_2 = 0.5, \gamma_3 = 0.0001$, $\sigma_1 = 2.2$, $\sigma_2 = 2$, $\sigma_3 = 0.05$, $\omega = 0.05$, $\xi = 871500$. The observer gain $K = [k_1, k_2]^T = [2,5]^T$ is selected, and the matrix $Q = diag[6,6]$ is defined such that $\lambda_{\min}(Q) - 11/2 > 0$. Using equation (25), the matrix $P = \begin{bmatrix} 18 & -6 \\ 6 & 6 \end{bmatrix}$ is obtained. The sensor fault parameters are set to $\mu = 0.4$, $T_{f1} = 30s$. The actuator fault parameters and functions are set to $\beta = 0.8$, $\bar{u} = 0.1(1 - e^{-0.5t})$, $T_{f2} = 50s$. The given ideal tool surface signal is $y_d = 0.7\pi \sin(0.2t)$. The flow rate is set to $Q(t) = 36 + 20\cos(0.25t)L/S$.

ISSN: 2688-8645

The simulation results are shown in Figures 4 to 9. Figure 4 compares the tracking performance of the system output tool face angle with the fault compensation control method proposed in this paper and the system output tool face angle without fault compensation. The blue dashed line represents the tracking curve of the fault compensation method, and the black solid line represents the tracking curve of the method without fault compensation. It can be seen that the proposed control method ensures that the system output trajectory can still track the reference signal after sensor and actuator faults occur, whereas the method without fault compensation cannot achieve the desired tracking performance. Figure 5 shows the control input signal conditions. Under this control input, the system can quickly and stably track the set tool face angle. Figure 6 shows the observation results of the fuzzy state observer. It can be seen that even under sensor fault conditions, the fault compensation control method can still maintain good observation performance. Figure 7 shows the variation curve of the adaptive compensation parameters. Figures 8 and 9 show the tracking error curves of the control methods with and without fault compensation. The tracking error of the fault-compensated control converges quickly to a small neighborhood near the origin.

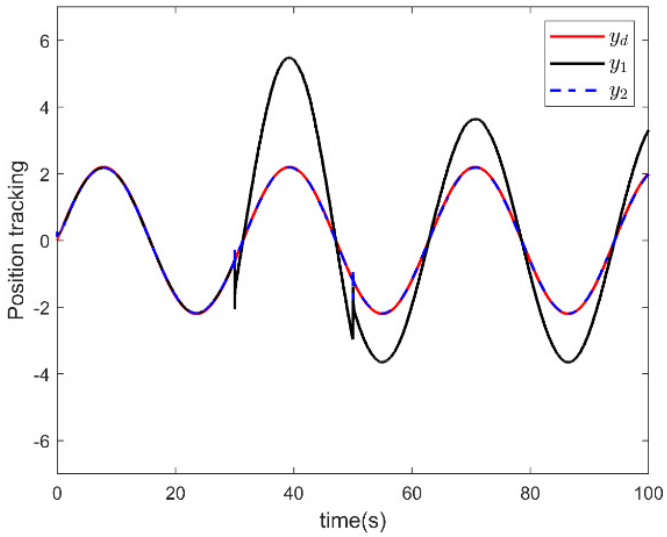

Figure 4. Tool surface tracking trajectories under two control methods

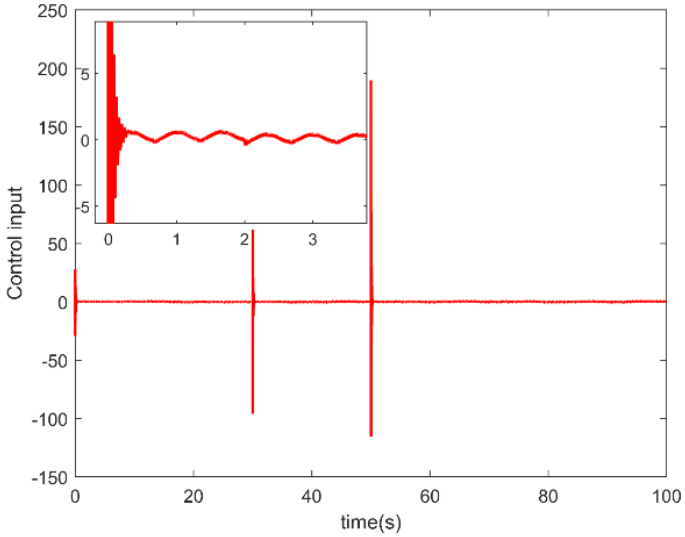

Figure 5. Control input signal

ISSN: 2688-8645

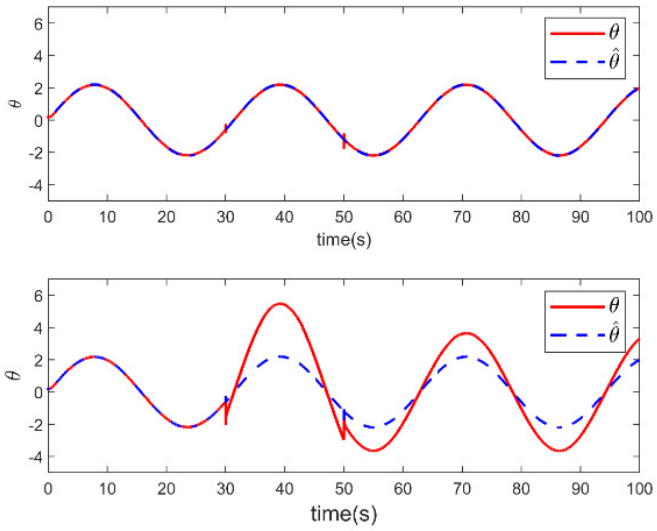

Figure 6. Tool face angle and its observed value under two control methods

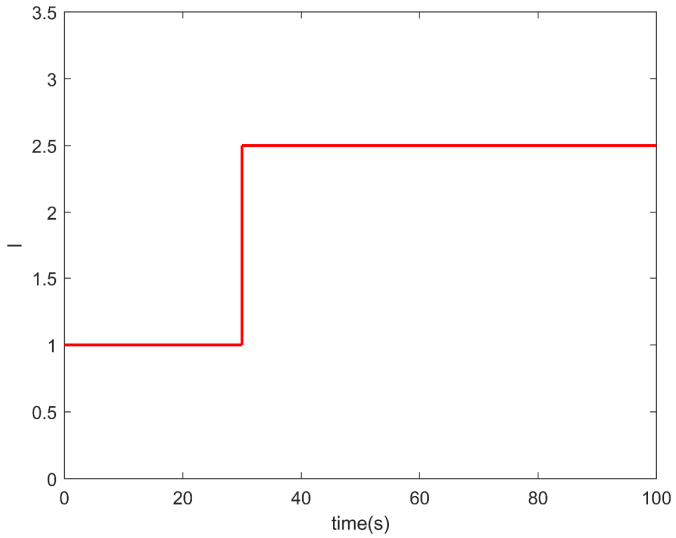

Figure 7. Adaptive law $\hat{l}$

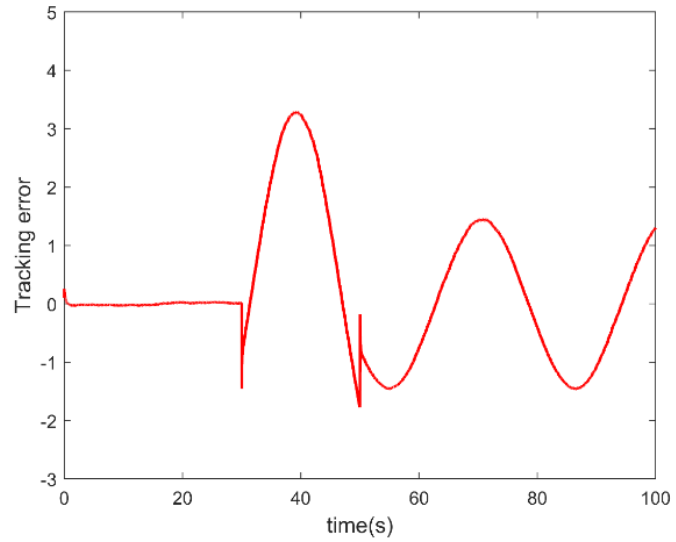

Figure 8. Tracking error of fault-free compensation method

ISSN: 2688-8645

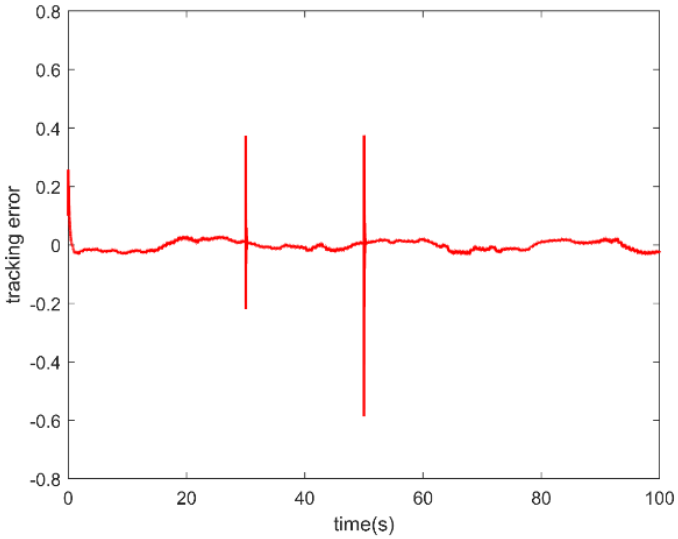

Figure 9. Tracking error of fault compensation method

6. Conclusion

This paper proposes a fuzzy adaptive finite-time control scheme for the stable platform of a Rotary Steerable System (RSS) subject to sensor and actuator faults. The scheme integrates backstepping control with finite-time control techniques. Specifically, a fuzzy state observer equipped with an adaptive fault compensation mechanism is developed to estimate unmeasurable state variables. By constructing an appropriate Lyapunov function, adaptive laws for the fault parameters are derived. This compensation method effectively mitigates the adverse effects of sensor faults, thereby guaranteeing the system's tracking performance. Furthermore, a novel controller is designed to achieve finite-time convergence, ensuring that the tracking error is confined to a small neighborhood of the origin. Finally, simulation experiments validate the effectiveness and robustness of the proposed algorithm.

References

[1] Wei L I, Lei M O U, Xiancheng Z, et al. Research progress of rotary steerable system and its control methods[J]. Coal Geology & Exploration, 2023, 51(10): 167-179.

[2] Zhang LG, Liu GR, Li W, et al. Analysis and optimization of control algorithms for RSSTSP for horizontal well drilling[J]. Journal of Petroleum Exploration & Pro- duction Technology, 2018, 8(4): 1069-1078.

[3] Zhang C, Zou W, Cheng N, et al. Adaptive fault-tolerant control for trajectory tracking and rectification of directional drilling. Int J Control Autom 2022; 20(1): 334–348.

[4] Wang G, Huang W, Gao D. Real-time control algorithm of well trajectory for push-the-bit rotary steering drilling system[J]. SPE Journal, 2023, 28(05): 2148-2164.

[5] Sheng L, Niu Y, Wang W, et al. Estimation of toolface for dynamic point-the-bit rotary steerable systems via nonlinear polynomial filtering. IEEE Trans Ind Electron 2022; 69(7): 7192–7201.

[6] Zhang N, Li F, Ren B, et al. Research on wellbore trajectory control of Rotary Steerable System using back-propagation neural network-fuzzy method[J]. Geoenergy Science and Engineering, 2025: 214201.

[7] Wang G, Huang W, Gao D. Real-time control algorithm of well trajectory for push-the-bit rotary steering drilling system[J]. SPE Journal, 2023, 28(05): 2148-2164.

[8] Ji C, Dong M, Yu D, et al. A sliding mode control based stabilization method for directional rotary steering tool-face[J]. Tehnički vjesnik, 2023, 30(3): 930-936.

[9] Wang H, Kang Y, Yao L, et al. Fault diagnosis and fault tolerant control for T–S fuzzy stochastic distribution systems subject to sensor and actuator faults[J]. IEEE Transactions on Fuzzy Systems, 2020, 29(11): 3561-3569.

[10] Li S, Wang Y, Wu X, et al. Self-Stabilizing Control Strategy of Stabilized Platform for Rotary Steerable Drilling System Based on Adaptive Backstepping Control[C]//Actuators. MDPI, 2024, 13(3): 116.

[11] Wang Y, Fei W, Huo A, et al. Electromagnetic torque feed-forward control of the turbine alternator for rotary steering drilling tools. Acta Pet. Sin. 2014, 35, 141–145.

[12] Wu T, Yu Z, Li S. Observer-based adaptive fuzzy quantized fault-tolerant control of nonstrict-feedback nonlinear systems with sensor fault[J]. IEEE Transactions on Fuzzy Systems, 2022, 31(6): 1900-1911.

[13] Tong S, Min X, Li Y. Observer-based adaptive fuzzy tracking control for strict-feedback nonlinear systems with unknown control gain functions[J]. IEEE Transactions on Cybernetics, 2020, 50(9): 3903-3913.

[14] Yu J, Zhao L, Yu H, et al. Fuzzy finite-time command filtered control of nonlinear systems with input saturation[J]. IEEE Transactions on Cybernetics, 2017, 48(8): 2378–2387.

[15] Wang LX. Stable adaptive fuzzy control of nonlinear systems. IEEE Trans Fuzzy Syst 1993; 1(2): 146–155.

[16] Wang LX. Adaptive fuzzy systems and control: design and stability analysis. Englewood Cliffs: Prentice-Hall, Inc, 1994.